7-2008

The 5 GHz Airport Surface Area Channel: Part II, Measurement and Modeling Results for Small Airports

Indranil Sen

David W. Matolak
University of South Carolina - Columbia, matolak@cec.sc.edu

Publication Info

Postprint version. Published in *IEEE Transactions on Vehicular Technology*, Volume 57, Issue 4, 2008, pages 2027-2035.

The 5-GHz Airport Surface Area Channel—Part II: Measurement and Modeling Results for Small Airports

Indranil Sen, *Member, IEEE*, and David W. Matolak, *Senior Member, IEEE*

***Abstract*—This paper describes results from a channel measurement campaign performed at several small airports in the U.S. in the 5-GHz band. This paper is a companion to another paper, which describes channel models for large airports. We classify the small airport surface channel into three propagation regions based upon different delay dispersion conditions. The channel characteristics of these regions in the delay and frequency domains are discussed with examples. We provide empirical stochastic channel models (of different bandwidths) to accurately represent the channel on the airport surface area for all propagation regions. The models are provided in the form of tapped delay lines, and complete statistical tap descriptions are given. Several key observations, including the presence of severe amplitude fading, some correlated scattering, and statistically nonstationary behavior, are also discussed.**

***Index Terms*—Channel impulse response (CIR), fading, radio propagation.**

I. Introduction

As THE 21st century proceeds, the number of people using airplanes has been dramatically increasing. It is a priority of major airlines to provide improved and affordable air travel. Air-freight activities have also been increasing. The increase in the demand for air travel affects organizations such as airlines, transportation and security groups, and catering agencies that work within the airport surface boundaries. The activities of these organizations need to be well coordinated, and additional communication services will be needed to ensure efficiency, safety, and security [1]. The number of small aircraft (personal and business) has been increasing as well.

As noted in [2], with an increase in the number of airplanes, there is decreased spectral resource availability in the near-saturated aeronautical very-high-frequency (VHF) band. This creates an urgent need to consider other available spectral regions for new applications. In view of this, the National Aeronautics and Space Administration's Glenn Research Center's Advanced CNS Architectures and Systems Technologies (ACAST) program was conducted to begin investigations to improve airport surface communications [3]. Another option being researched is the optimal usage of existing (VHF) spectrum. Under this, relatively new and popular multicarrier modulation techniques have been proposed in [4].

In addition, as described in [2], the aeronautical frequency band from 5.091 to 5.15 GHz—the "microwave landing system extension" band (E-MLS)—is currently underutilized in much of the world and is expected to remain so. Thus, this band is attractive for development and deployment of new short-range wireless systems [5].

In [2], we described pertinent related references for the aeronautical and airport surface channels [6]–[10]. Throughout this paper, see [2] for underlying theory and details, and in this second part, we highlight the key and distinguishing features germane to *small* airport surface area channels. We include discussions of propagation area classification, channel parameters, etc., as needed to maintain clarity and keep this part mostly self-contained.

To motivate our work, we note that the MLS band carrier frequency allows for the use of wider channel bandwidths than at VHF, and hence, wideband stochastic models are needed. Other than [10], all cited work for the airport surface channel has either been narrowband, restricted to line-of-sight (LOS) conditions, or deterministic, further motivating our work.

For our research on the "ground-to-ground" (GG) airport surface channel, we are interested in the areas that include only the "taxi" and "parking" scenarios from [10]. The models proposed in [10] are based on analogy with corresponding terrestrial cellular regions (e.g., urban and rural). To the best of our knowledge, [10] is the only existing work for wideband GG channel models at airports. The underlying assumptions (based on cellular models) and limited use of corroborating empirical data further warrant development and use of our new models presented here and in [11].

We completed a measurement and modeling campaign to characterize the airport surface channel in the E-MLS band. The first part of our results is presented in [2], which covers channel models for large airports. In this paper, we concentrate on the smaller general aviation (GA) airports. Section II summarizes measurements, Section III describes channel models, and Section IV contains conclusions.

Manuscript received August 3, 2006; revised January 31, 2007, May 22, 2007, and September 13, 2007. This work was supported by the National Aeronautics and Space Administration (NASA) under Grant NNC04GB45G. The review of this paper was coordinated by Dr. W. Zhuang.

I. Sen was with the School of Electrical Engineering and Computer Science, Ohio University, Athens, OH 45701 USA. He is now with Motorola Inc., Libertyville, IL 60048 USA (e-mail: indranil.sen@motorola.com).

D. W. Matolak is with the School of Electrical Engineering and Computer Science, Ohio University, Athens, OH 45701 USA (e-mail: matolak@ohiou.edu).

Color versions of one or more of the figures in this paper are available online at http://ieeexplore.ieee.org.

Digital Object Identifier 10.1109/TVT.2007.912335

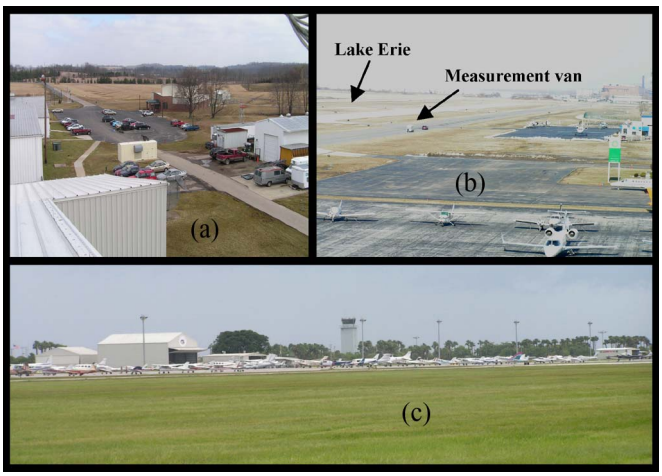

Fig. 1. Photographs from different GA airports. (a) Ohio University. (b) Burke Lakefront. (c) Tamiami.

II. Measurement Summary

A. Airport Descriptions

GA airports are generally used and frequented by aircraft that are much smaller than those encountered at larger (i.e., medium or large [2]) airports. Aircraft commonly seen at GA airports are single- and twin-propeller aircraft. For our measurement campaign, the choice of airports was based on accessibility and geographic location. The first set of measurements was made at the Ohio University (OU) Airport. Fig. 1(a) shows a view from the "crow's nest" on the roof of a hangar at the OU airport. We used the "crow's nest" as the transmitter location since it was the tallest accessible structure at the airport. The OU airport has only a few buildings on the airport property, including buildings that belong to the OU School of Aviation, the Avionics Engineering Center, and the airport terminal itself. In addition to these buildings are hangars and equipment sheds. Some of these structures are visible in Fig. 1(a). Measurements on the OU airport were made during February and March 2005. Another feature for the OU airport is the proximity of U.S. Route 33 on one side of the airport perimeter. The presence of vehicular traffic on this route sometimes caused long delay multipath components.

The second set of measurements was made at Burke Lakefront (BL) airport in Cleveland, OH. The proximity of BL to downtown Cleveland, with Lake Erie on the other side, created an interesting geographic location. Some long delay multipath reflections from the large downtown buildings were observed. In fact, the majority of the scatterers at BL were concentrated on the downtown side of the air traffic control tower (ATCT). As with other GA airports, BL has a few buildings on the airport property and is used by smaller airplanes. The measurements at BL were made at the end of March 2005. Fig. 1(b) is an example photograph taken from the BL ATCT. The measurement vans, Lake Erie, and some of the parked airplanes can be seen in this picture, with our receiving measurement van seen moving on the runway.

The final set of GA airport channel measurements was made at Tamiami (TA) airport, Kendall, FL. The TA airport is among the biggest GA airports in the U.S. At TA, we were unable to place our transmitter on the ATCT and, instead, used the roof of an instrument landing system (ILS) shed as the transmitter location. Due to the relatively low height of the ILS shed (approximately 4 m), larger airport surface area, and larger number of airplanes on the surface, our TA channel has a scattering geometry that is significantly different from the other GA airports. Fig. 1(c) is a photograph of the airport surface area taken from the ILS shed, in which the ATCT, some hangars, and quite a few aircraft parked on the surface can be seen. The TA airport also has a service road that runs on the outskirts of the airport property. Fig. 2 provides a diagram of the measurement route taken at TA. The numbers within the circles are the locations that designate starting/stopping points on the airport surface. As with the large airport measurements, the travel route selection was made to ensure coverage of all possible airport surface locations to sample all the different signal propagation conditions. To account for effects of transmitter location on channel characteristics (at large airports), we developed additional models [11], [12].

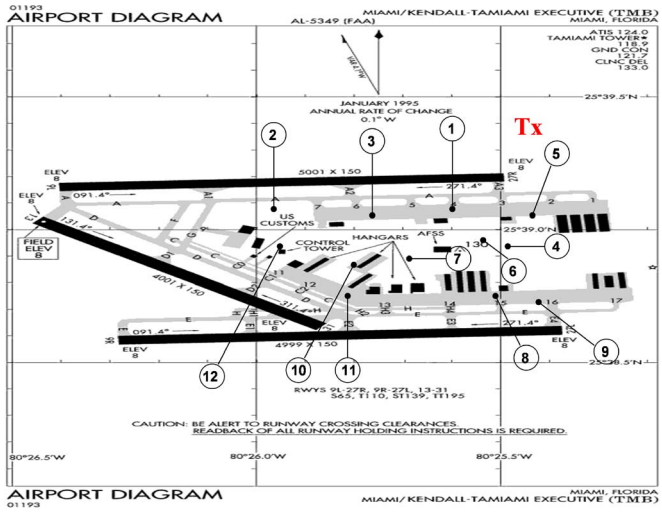

Fig. 2. Measurement route taken at TA.

The main differences between the GA airports and the large/medium airports described in [2] are the smaller height of the ATCT (the ATCT height for BL is ∼15 m, and that for OU is ∼10 m), the smaller airport surface area, the smaller plane sizes, the smaller size and number of buildings on the airport property, and a generally smaller number of ground vehicles that are present on the airport surface. Link distances were less than 2 km. Due to these differences in the physical environment, it is obvious that separate GA airport channel models are warranted. In the following sections, as we discuss measurement results, we highlight other salient differences in the fading characteristics encountered at the small and large airports.

B. Equipment Description and Data Preprocessing

Our data collection method is similar to the one described in [13] and [14]. We use a fairly wideband channel "sounder" with 20-ns delay resolution: It is a modified version of the "Raptor" spread spectrum stepped correlator by Berkeley Varitronics

Systems, Inc. [15]. This sounder enables measurement and subsequent statistical characterization of the channel impulse response (CIR) and propagation path loss. For more details regarding the test equipment, see [3] and [11]. The sounder measurements suffer from inherent systematic errors, a discussion of which is presented in [16]; as we note in [2], these errors are inconsequential for our measurements.

Data preprocessing to account for the channel sounder's autocorrelation and for noise is also described in [2]. The thresholding method that we used for noise reduction is the same as that in [17]. The thresholding ensures that the probability of mistaking a noise spike for an actual channel impulse is approximately 10^{-3} for any given power delay profile (PDP). The antennas used for the measurement campaign were omnidirectional monopoles, above ground planes (with radome), and have gain $\sim$1.5 dBi. The PDP readings were logged in a laptop computer, which is connected to the sounder receiver unit via a serial RS-232C port. In addition, both the transmitter and receiver units have GPS receivers and antennas, which can be used for distance determination.

C. Region Classification and Collected Data Summary

As with the airport size classification, we have classified the airport channel regions into a set of three as follows: 1) LOS-Open (LOS-O); 2) NLOS-Specular (NLOS-S); and 3) NLOS. For these three regions (the same as used for the large/medium airports [2]), the LOS-O areas are those that are clearly visible from the ATCT, with no significant scattering objects nearby, e.g., runways and some taxiways. The NLOS-S regions represent the regions in between the other two and exhibit mostly NLOS conditions but with a noticeable, often dominant, specular, or first-arriving component in the PDP, in addition to lower energy multipath components. The NLOS regions represent areas of the airport that have a completely obstructed LOS to the ATCT.

One of the most popular methods of quantifying channel time dispersion is the root mean square delay spread (RMS-DS). The RMS-DS for a PDP is calculated in the usual way [18] as

$$\sigma_\tau = \sqrt{\frac{\sum_{k=0}^{L-1} \tau_k^2 \alpha_k^2}{\sum_{k=0}^{L-1} \alpha_k^2} - \mu_\tau^2} \tag{1}$$

where the α's and τ's are the amplitudes and delays, respectively, of the measured multipath components, and the mean energy delay μ_τ is given by

$$\mu_\tau = \frac{\sum_{k=0}^{L-1} \tau_k^2 \alpha_k^2}{\sum_{k=0}^{L-1} \alpha_k^2}. \tag{2}$$

We use the RMS-DS to separate the PDPs into different regions. Figs. 3 and 4 show histograms for the RMS-DS collected at BL and TA. The following two things stand out: 1) the presence of multiple propagation regions (non-uni-modal probability density functions) and 2) the higher dispersion at TA.

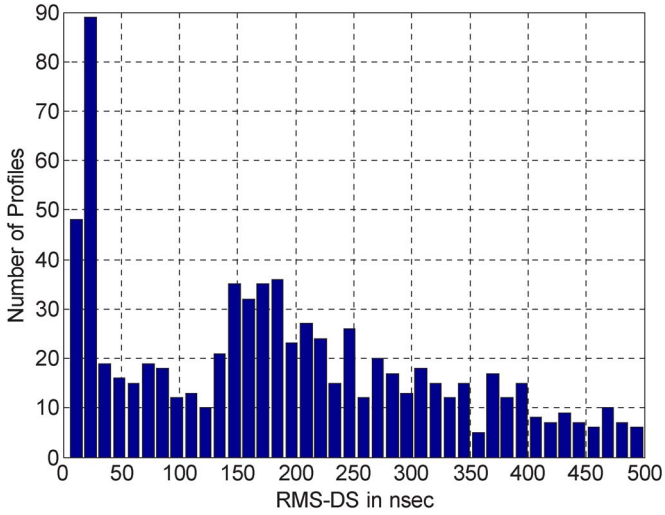

Fig. 3. Histogram of measured RMS-DS at BL.

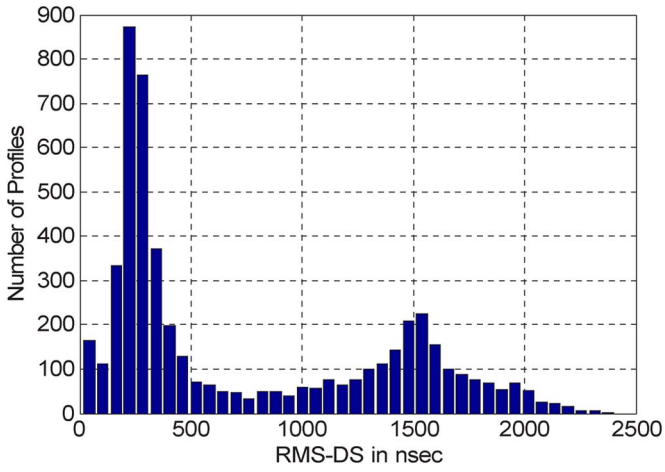

Fig. 4. Histogram of measured RMS-DS at TA.

TABLE I
SUMMARY OF MEASURED PDPS FOR EACH PROPAGATION REGION

AIRPORT (TOTAL # PDPS)	TOTAL # PDPS IN EACH REGION		
	NLOS (σ_{t2}, NS)	NLOS-S (σ_{t1}, NS)	LOS-O
BL (1108)	—	652 (125)	256
OU (908)	—	1,108	—
TA (5203)	2,248 (500)	2,955	—

Based upon a visual inspection of the BL scattering environment, the portion of the BL airport surface area with NLOS conditions was small; these observations are corroborated by the RMS-DS distribution, which shows a relatively small fraction of large RMS-DS values. Thus for BL, we have only LOS-O and NLOS-S regions.

For TA, due to the reduced transmitter height and a much larger airport surface area, TA has two distinct regions: 1) NLOS-S and 2) NLOS. Table I shows the number of PDPs collected at the different airports for different regions. We also provide values of RMS-DS used as thresholds to distinguish

TABLE II
SUMMARY OF MEASURED RMS-DS VALUES FOR THREE AIRPORTS

AIRPORT	RMS-DS (NS) [MIN; MEAN; MAX]		
	NLOS	NLOS-S	LOS-O
BL	—	[126; 429; 2,427]	[5; 44; 124]
OU	—	[14; 293; 2,416]	—
TA	[502; 1,390; 2,404]	[15; 256; 499]	—

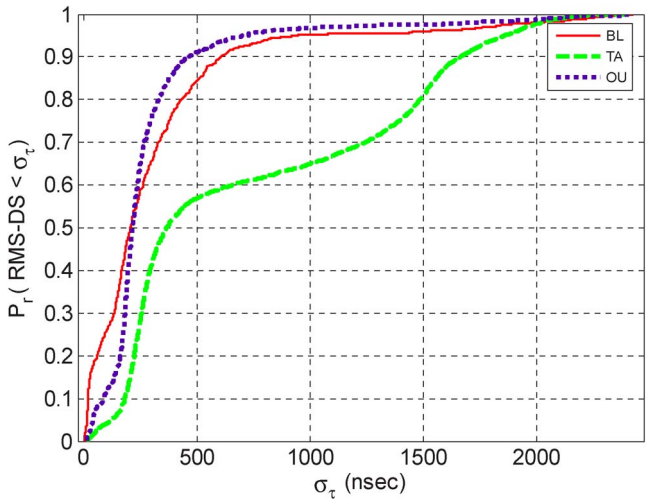

Fig. 5. Cumulative distribution functions of RMS-DS for three GA airports.

TABLE III
SUMMARY OF COMPUTED FCE VALUES FOR THREE REGIONS

AIRPORT	FCE (MHZ) FOR CORRELATION OF [0.9; 0.5; 0.2]		
	NLOS	NLOS-S	LOS-O
BL (1108)	—	[3.5; 13.2; 19.6]	[6.6; 16 ; 21.4]
OU (908)	—	[3.9; 12.5; 21.4]	—
TA (5203)	[NA; 9; 16]	[3.9; 14.1; 20.8]	—

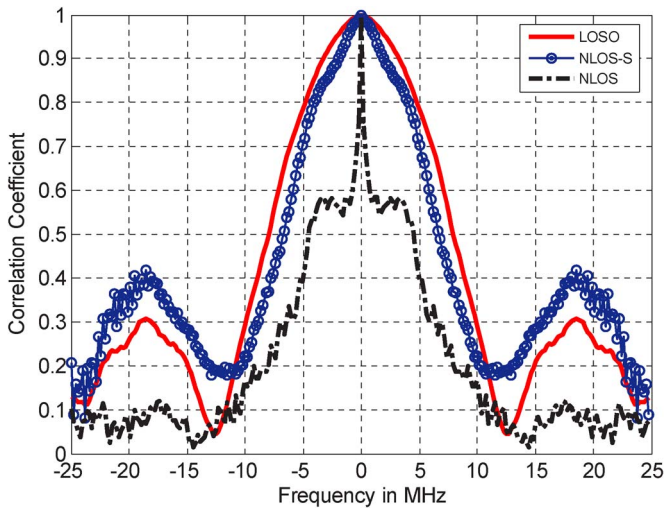

Fig. 6. Example FCEs for different GA airport propagation regions.

regions. The choice of the thresholds $\sigma_{\tau x}$ is based on the distribution of the RMS-DS, where subscript "x" is 1 for the threshold between LOS-O and NLOS-S and is 2 for that between NLOS-S and NLOS.[1] Note that for large airports, aircraft will generally inhabit all three regions as they taxi around the airport surface, but in the case of small airports, aircraft may or may not encounter different regions. There are though GA airports (e.g., TA) where one could encounter all the different propagation regions, and due to the presence of these different regions, the channel can be statistically nonstationary over fairly short durations (tens to hundreds of milliseconds). This nonstationarity is typically not accounted for in other terrestrial channel models but is something that we model here. In addition, as noted in [2] for large airports, scattering is essentially *never* isotropic about the mobile ground vehicle.

In Table II, we list summary values of measured RMS-DS: mean, maximum, and minimum. Fig. 5 shows the cumulative distribution function (cdf) of RMS-DS for the three airports. For BL and OU, the 50th percentile values are very close to 200 ns, whereas for TA, with its lower transmitter height, the 50th percentile value is closer to 400 ns. These values are much smaller than the 50th percentile values seen at medium and large airports (approximately 500–1000 ns), [2]. Only the low-Tx-elevation TA measurements yielded larger 90th percentile RMS-DS values. The steep rise of the RMS-DS cdf for OU and BL suggests that the channel is less frequency selective (than at TA), yet due to their proximity to US-33 and downtown Cleveland, respectively, there were a small percentage of higher valued RMS-DS PDPs for those airports.

To quantify the effect of channel dispersion in the frequency domain, we use the frequency correlation estimate (FCE), which is analogous to the coherence bandwidth [18]. We cannot always assume the classical wide sense stationary-uncorrelated scattering (WSSUS) environment due to nonstationarity [19] and correlated scattering (discussed subsequently). We thus use the formula from [20] to compute the FCE. In this method, time variations of different spectral components are directly cross-correlated with the time variations of the component at a reference frequency. See [2] for computation details.

Table III lists bandwidths for which the frequency correlation takes the values of 0.9, 0.5, and 0.2. The bandwidth values that we cite are associated with the smallest frequency separation for which the FCE attains the correlation value. For the NLOS case, due to our frequency resolution limit (255 points in 50 MHz for approximately 196 kHz per frequency bin), we cannot easily determine the frequency separation for which the FCE reaches 0.9. Example FCEs for the three regions are shown in Fig. 6. As expected, the width of the main lobe for LOS-O is largest, followed by NLOS-S, then NLOS.

[1]As noted in [2], small changes in the values of these thresholds will not appreciably change results.

III. Channel Models

In this section, we provide a discussion regarding the channel parameters that are needed to develop channel models for different regions of the GA airports. Complete channel models for two values of channel bandwidth are then presented. Unless otherwise noted, the plots, tables, and parameters pertain to a 50-MHz bandwidth.

A. Nonstationary CIR Model

For most cases in the literature, as well as in our research, we represent the channel as a linear time-varying filter that is characterized completely by its impulse response. The impulse response is defined as the function $h(\tau;t)$, which is the response of the channel at time t to an impulse input at time $t-\tau$

$$h^{(e)}(\tau;t) = \sum_{k=0}^{L(t)-1} z_k(t)\alpha_k(t)\exp\{j\left[\omega_{D,k}(t)\left(t-\tau_k(t)\right) - \omega_c\tau_k(t)\right]\}\delta\left[\tau-\tau_k(t)\right] \quad (3)$$

where, at time t, $\alpha_k(t)$ represents the kth resolved amplitude, and the argument of the exponential term is the kth resolved phase. The kth multipath component has a time-varying delay $\tau_k(t)$, the δ-function is a Dirac delta, the radian carrier frequency is $\omega_c = 2\pi f_c$, and the term $\omega_{D,k}(t) = 2\pi f_{D,k}(t)$ represents the Doppler shift associated with the kth resolved multipath component, where $f_{D,k}(t) = v(t)f_c\cos[\theta_k(t)]/c$, where $v(t)$ is the relative velocity, $\theta_k(t)$ is the aggregate phase angle of all components arriving in the kth delay bin, and c is the speed of light. The kth resolved component consists of multiple terms from different spatial angles $\theta_{k,i}$ received in the kth delay bin.

In (3), we have generalized the CIR beyond that typically seen in texts [18] to allow for 1) an "environment" classification (superscript "e" on h) to denote CIRs for the various airport regions and 2) a "persistence process" $z(t)$ to account for the finite "lifetime" of propagation paths. The time-varying number of transmission paths (line of sight and/or multipath echoes) $L(t)$ arises naturally from the persistence process. The persistence process is used to account for the finite "lifetime" of scatterers that contribute to the multipath components.

We model the persistence process using a first-order Markov chain. The first step in specifying the Markov process for any given multipath component (channel tap) is to identify the ON/OFF states from the data. We declare the presence of multipath in a delay bin ($z_k(t) = 1$, ON) whenever the amplitude is within 25 dB of the maximum amplitude in the PDP. Collecting z_k samples across time yields a series of 1s and 0s (0, OFF), which model the persistence process for that particular delay bin. As with all Markov processes, the persistence process for any bin has an associated transition (TS) matrix and steady-state probability vector (SS). An example TS matrix for tap 5, NLOS region, is given in (4), and the corresponding tap SS vector is provided in (5). Each element P_{ij} in matrix TS is defined as the probability of going from state i to state j,

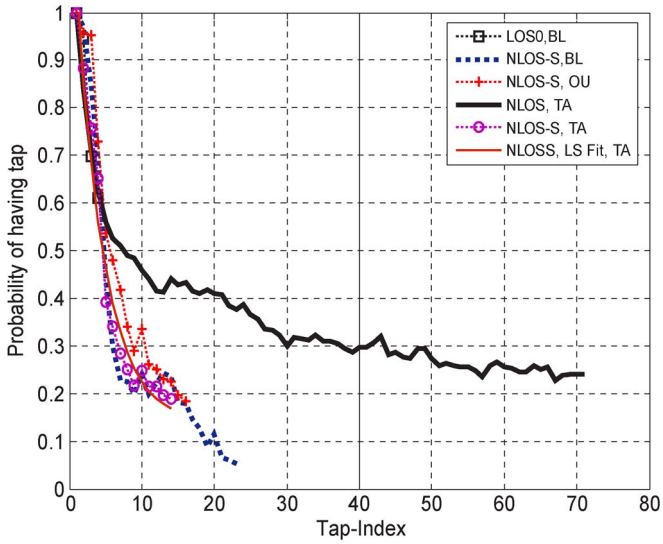

Fig. 7. Steady-state tap probability for state 1 (tap "ON") versus tap index: BL, OU, and TA and NLOS, NLOS-S, and LOS-O.

and each SS element P_j gives the "steady-state probability" associated with the jth state as follows:

$$TS_5^{(\mathrm{NLOS})} = \begin{bmatrix} P_{00} & P_{01} \\ P_{10} & P_{11} \end{bmatrix} = \begin{bmatrix} 0.6475 & 0.3525 \\ 0.4526 & 0.5474 \end{bmatrix} \quad (4)$$

$$SS_5^{(\mathrm{NLOS})} = \begin{bmatrix} 0.4371 \\ 0.5679 \end{bmatrix}. \quad (5)$$

For CIR modeling, we obtained the SS elements for tap persistence as the "fractions of time" that the multipath components are either present ($z_k(t) = 1$) or not ($z_k(t) = 0$), directly from all the PDP data of a given region; the TS elements were similarly empirically derived. The persistence process is different from the small-scale fading process due to the longer memory associated with the persistence process. The parameters of the persistence process are mainly influenced by the physical dimensions of the scatterers and reflectors, the velocity of the transmitting and receiving platforms, etc.

Fig. 7 shows the measured tap probability of occurrence (Pr ["ON"]) versus tap index (20 ns), illustrating the strong similarity of NLOS-S statistics for the three different GA airports. Least-squares curve fits for these probability of occurrence curves fit the general form

$$P(k) = c_0\exp(-c_1 k) + c_2 \quad (6)$$

where k is the tap index, and the c's are curve fit constants. Table IV lists these constants for the airports and regions. For clarity, only one curve fit appears in Fig. 7. As expected, the tap probability of occurrence for higher index NLOS taps is greater than that in the NLOS-S case.

The time-varying amplitude associated with each tap can be modeled using different statistical distributions. The parameters for these statistical distributions for each tap are determined using all PDP data (with tap persistence $z(t) = 1$), using the maximum likelihood criterion. In general, the best fit was obtained, for the largest number of taps, using the Weibull

TABLE IV
LEAST SQUARES FIT PARAMETERS FOR TAP PROBABILITY OF OCCURRENCE (6)

AIRPORT	EQ. (6) LS FIT PARAMETERS $[C_0; C_1; C_2; K_{MAX}]$		
	NLOS	NLOS-S	LOS-O
BL	—	[1.2697; 0.2374; 0.1013; 23]	[7.1159; 0.0209; -5.9409; 4]
OU	—	[1.1799; 0.1761; 0.1015; 6]	—
TA	[0.6185; 0.1007; 0.2729; 71]	[1.1966; 0.2598; 0.1368; 4]	—

TABLE V
FIRST TAP RICEAN k-FACTORS AND RANGE OF WEIBULL β-FACTORS

AIRPORT	K-FACTORS (DB); RANGE OF β-FACTORS [MIN; MAX]		
	NLOS	NLOS-S	LOS-O
BL	—	12.5 (1.7; 2.73)	14.5 (1.88; 2.4)
OU	—	8.9 (1.75; 2.36)	—
TA	(1.4; 1.87)	11 (1.54; 2.02)	—

distribution [21]. Like the Nakagami-m model, the two-parameter Weibull density offers flexibility, i. e.,

$$p_W(x) = \frac{\beta}{\alpha^\beta} x^{\beta-1} \exp\left[-\left(\frac{x}{a}\right)^\beta\right] \tag{7}$$

where β is a shape factor that determines fading severity, $a = (\Omega/\Gamma[(2/\beta)+1])^{1/2}$ is a scale parameter, in which $\Omega = E(x^2)$, and Γ is the gamma function. A value of $\beta = 2$ yields the well-known Rayleigh distribution, and $\beta < 2$ denotes more severe fading. The number of taps changes as a function of the channel bandwidth. In Section III-B, we provide tap statistics for two bandwidths of current interest, based on contemporary communication system standards.

Table V summarizes tap amplitude statistic results with values for the Ricean K-factor for the first tap in the LOS-O and NLOS-S settings, and the range of the Weibull factor β, across *all* remaining taps (other than the first) for the LOS-O and NLOS-S settings. For the NLOS setting, the Weibull β parameter applies to all taps. The Ricean K-factor values were computed using the ML fit to all data in all airports for the given region. The minimum values of the Weibull β parameter are less than two, indicating severe fading. (Rayleigh fading has traditionally been associated with the worst-case fading conditions.) Figs. 8 and 9 illustrate example probability density function fits for the first two taps in the LOS-O region, showing, for the second tap, the severe fading represented by a Weibull β factor less than two. Severe fading occurs in most of our regions, and some of the explanations we posit for this are listed as follows (see also [2]):

1) A small number of multipath components per delay bin [22]: possible in nearly open airport areas like BL and OU, where, for much of the airport surface, we do not have rich scattering;
2) multiple scattering [23], [24];
3) Frequent channel transitions [25], which redistribute multipath energy among components so that a given component experiences worse than Rayleigh fading.

For more details on these fading mechanisms, see [25].

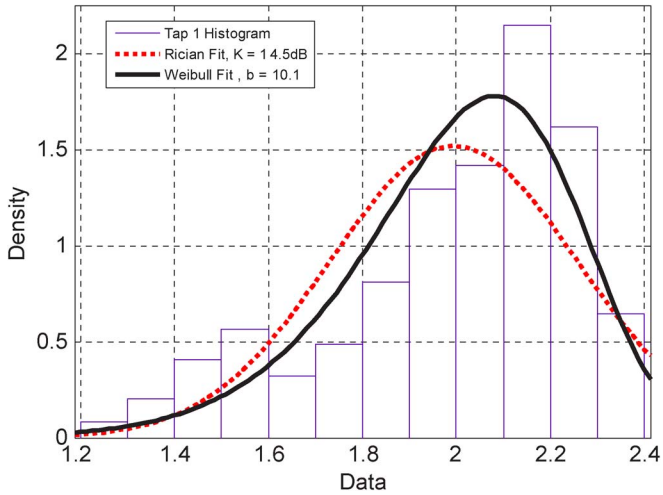

Fig. 8. Amplitude statistics of tap 1 for GA airport LOS-O regions.

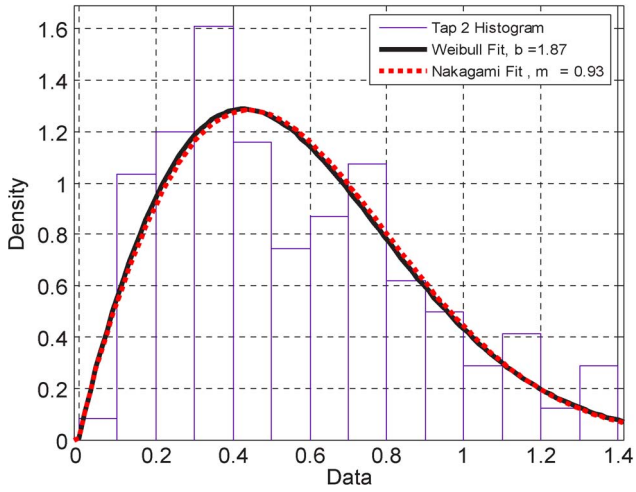

Fig. 9. Amplitude statistics of tap 2 for GA airport LOS-O regions.

B. Models for Several Channel Bandwidths

In this section, we provide channel models for two values of bandwidth: 10 and 5 MHz. As noted, selection of bandwidth values was based upon those for wireless technologies that are likely to be used in the airport surface environment [26], [27]. For channel models for additional bandwidths, see [3] and [11].

The first step in creating the channel model is the determination of the number of taps, and this was done according to the mean RMS-DS, i.e., the number of taps L for a 50-MHz model is

$$L = \lceil E(\sigma_\tau)/T_c \rceil + 1 \tag{8}$$

TABLE VI
NUMBER OF TAPS FOR SMALL AIRPORT CHANNEL MODELS WITH DIFFERENT BANDWIDTHS

BANDWIDTH (MHZ)	AIRPORT	NLOS-S (99% ENERGY)	NLOS (95% ENERGY)	LOS-O (99% ENERGY)
50	OU	8	—	—
	BL	10	—	2
	TA	5	36	—
20	OU	2	—	—
	BL	4	—	2
	TA	4	18	—
10	OU	2	—	—
	BL	2	—	2
	TA	2	10	—
5	OU	2	—	—
	BL	2	—	2
	TA	2	6	—
1	OU	2	—	—
	BL	2	—	2
	TA	2	2	—

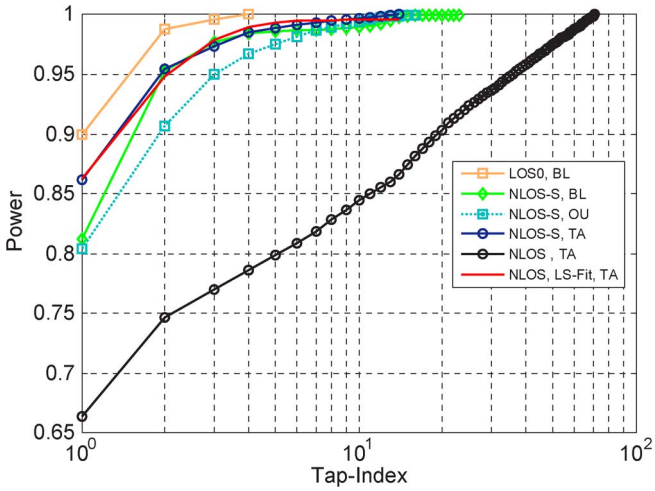

Fig. 10. Cumulative energy versus tap index for all GA airports regions.

where σ_τ is the RMS-DS, the "E" operator denotes expectation, and T_c is our chip time of 20 ns. Determination of the number of taps for bandwidths of 10 and 5 MHz is done by vectorially combining five and 10 chip samples, respectively. Table VI provides the numbers of taps for several bandwidths, for the LOS-O, NLOS-S, and NLOS regions, for all three airports.

The number of taps for the channel model can also be based upon other parameters such as the maximum RMS-DS, yet for this extreme, there would be few PDPs from which to create statistics. The use of thresholding to limit the number of multipath components has also been used in the channel modeling literature [28]–[30]. As with large/medium airport results and as applies to our use of RMS-DS thresholds for propagation region classification, using a multipath threshold value larger than 25 dB resulted in insignificant changes to RMS-DS statistics (few nanoseconds), frequency correlations (less than 1 MHz), and numbers of channel taps (one or zero) [11].

The use of a threshold alone for determining the number of taps also does not take into account the relative tap energies.

TABLE VII
LEAST SQUARES FIT PARAMETERS FOR CUMULATIVE ENERGY (9)

AIRPORT	EQ. (9) LS FIT PARAMETERS [C_3; C_4; C_5]		
	NLOS	NLOS-S	LOS-O
BL	--	[0.7084; 1.3647; 0.0057]	[0.8624; 2.1636; 0.0010]
OU	--	[0.3712; 0.6836; 0.0053]	--
TA	[0.2779; 0.0555; 0.0053]	[0.3728; 1.0326; 0.0044]	--

TABLE VIII
CHANNEL PARAMETERS FOR 10-MHZ CHANNELS: SMALL AIRPORT

TAP INDEX K	ENERGY	WEIBULL SHAPE FACTOR (β_K)	$P_{1,K}$	$P_{00,K}$	$P_{11,K}$
NLOS					
1	0.714	2	1.0000	na	1.0000
2	0.073	1.42	0.8779	0.2549	0.8963
3	0.048	1.42	0.8123	0.3708	0.8550
4	0.041	1.42	0.7605	0.3848	0.8067
5	0.033	1.48	0.7419	0.4164	0.7973
6	0.022	1.59	0.6873	0.4509	0.7505
7	0.020	1.6	0.6662	0.4540	0.7268
8	0.017	2	0.6595	0.4563	0.7197
9	0.019	1.66	0.6753	0.4195	0.7213
10	0.014	2	0.6509	0.4547	0.7079
NLOS-S					
1	0.959	4.2	1.0000	na	1.0000
2	0.041	1.37	0.7276	0.5202	0.8200
LOS-O					
1	0.985	5.3	1.0000	na	1.0000
2	0.016	1.58	0.6593	0.6237	0.8045

TABLE IX
CHANNEL PARAMETERS FOR 5-MHZ CHANNELS: SMALL AIRPORT

TAP INDEX K	ENERGY	WEIBULL SHAPE FACTOR (β_K)	$P_{1,K}$	$P_{00,K}$	$P_{11,K}$
NLOS					
1	0.730	2.12	1.0000	na	1.0000
2	0.098	1.57	0.9162	0.2426	0.9306
3	0.064	1.49	0.8704	0.2824	0.8935
4	0.040	1.67	0.8004	0.3168	0.8300
5	0.037	1.68	0.7935	0.2608	0.8081
6	0.029	2	0.7639	0.3515	0.8000
NLOS-S					
1	0.959	4.22	1.0000	na	1.0000
2	0.041	1.41	0.6028	0.6996	0.8016
LOS-O					
1	0.986	5.15	1.0000	na	1.0000
2	0.014	1.58	0.5092	0.7744	0.7810

Considering the fairly large number of taps required to model the channel (Table VI), finding ways to reduce this complexity while maintaining model precision was our next step in model development. After finding L, we reduced the number of taps based upon cumulative energy, as implied by the column headings in Table VI. Fig. 10 shows the cumulative energy as a

TABLE X
CORRELATION COEFFICIENT MATRICES FOR 10-MHZ CHANNELS: SMALL AIRPORTS. LOWER TRIANGULAR PART: NLOS. UPPER TRIANGULAR PART: NLOS-S

i, j	1	2	3	4	5	6	7	8	9
1	1	*0.01*	—	—	—	—	—	—	—
2	0.27	1	—	—	—	—	—	—	—
3	0.24	0.03	1	—	—	—	—	—	—
4	0.34	0.26	0.13	1	—	—	—	—	—
5	0.24	0.21	0.11	0.41	1	—	—	—	—
6	0.18	0.20	0.03	0.13	0.28	1	—	—	—
7	0.24	0.16	0.13	0.15	0.23	0.05	1	—	—
8	0.09	-0.03	0.06	0.13	0.10	0.05	0.14	1	—
9	0.18	-0.01	0.14	0.14	0.13	0.09	0.11	0.04	1
10	0.17	0.06	-0.02	0.11	0.14	0.13	0.11	0.07	0.07

TABLE XI
CORRELATION COEFFICIENT MATRICES FOR 5-MHZ CHANNELS: SMALL AIRPORTS. LOWER TRIANGULAR PART: NLOS. UPPER TRIANGULAR PART: NLOS-S

i, j	1	2	3	4	5
1	1	*0.04*	—	—	—
2	0.25	1	—	—	—
3	0.29	0.26	1	—	—
4	0.09	0.20	0.16	1	—
5	0.12	0.04	0.14	0.16	1
6	0.13	0.12	0.08	0.10	0.11

function of tap index for all three airports and regions. Other than NLOS for TA, the curves flatten for the higher indexed taps. Thus, by not considering some of these higher index taps, we will not substantially affect the accuracy of the developed models. The logarithmic abscissa was used simply to separate the curves for clarity.

As with tap probability of occurrence, we also curve-fit tap cumulative energy as follows:

$$\mathrm{CE}(k) = 1 - c_3 \exp(-c_4 k) + c_5 \tag{9}$$

where, again, k is the tap index, with the range given in Fig. 10, and the fitting coefficients are given in Table VII. Tables VIII and IX provide the channel model parameters for the small airport 10- and 5-MHz channel models, respectively. The channel tap energies have been renormalized to account for the truncation (95% energy in NLOS and 99% energy in NLOS-S) so that the sum of all tap energies multiplied by their steady-state probabilities (P_1) equals unity. For the specific algorithm, see [2]. The Markov chain probabilities of Tables VIII and IX are defined in (4) and (5), with the remaining steady-state and transition probabilities found from the following relations:

$$P_0 = 1 - P_1, \quad P_{01} = 1 - P_{00}, \quad P_{10} = 1 - P_{11}.$$

The final step in developing the channel models is specification of tap correlation values. The tap correlation coefficient matrix for a given region is denoted by $R^{(\mathrm{region})} = [r_{i,j}]$, where $r_{i,j} = \mathrm{cov}(\alpha_\mathrm{i}\alpha_\mathrm{j})/(\mathrm{var}(\alpha_\mathrm{i})\mathrm{var}(\alpha_\mathrm{i}))^{1/2}$ is the correlation coefficient between taps i and j. We have computed these coefficients for short segments of travel (e.g., see Fig. 2) and over the entire set of data for a given region. Tables X and XI contain these correlation coefficient matrices, with NLOS and NLOS-S combined into one table, since only one half (upper or lower triangular part) of $R^{(\mathrm{region})}$ is unique. From these tables, we observe generally small positive correlations ($r_{i,j}$ from 0.2 to 0.4) between some taps for NLOS cases. Some worst-case correlation values above 0.6 were also observed [11]. In [11], we also provide a method for generating correlated Weibull random variables with arbitrary values of energy and fading parameters.

IV. SUMMARY AND CONCLUSION

In this paper, we have provided empirical stochastic channel models to accurately describe the physical propagation conditions at GA airports. These models are primarily useful in evaluating the performance of communication systems that would be deployed in the 5-GHz E-MLS band.

We provided descriptions of the different GA airports and compared the differences in the propagation conditions relative to large/medium airports [2]. Measurements were made with a 50-MHz bandwidth transmitter atop the 10–15-m-tall ATCTs and a receiver that travels in a mobile van on the airport surface. The difference in the scattering geometry and in the size and number of scatterers results in less dispersion for the GA airport channel than for the channel present at large/medium airports. Representative measurement results in the delay and frequency domains were provided. The GA airport channels do have some similarities with the large/medium airport channels, including the presence of severe fading, some correlated scattering in the nonisotropic scattering environment, and statistically nonstationary behavior.

Tapped delay line channel models for different bandwidths (5 and 10 MHz) were provided for the different propagation regions encountered on the GA airport surface. Amplitude statistics for the taps were provided using the Weibull distribution, and correlation coefficient matrices to model correlated scattering were also provided. The presence of severe fading was noted, and multiple possible mechanisms that lead to such behavior were given. This severe fading can be quantified as having a Weibull parameter $\beta \cong 1.5$, which is roughly equivalent to a Nakagami-m factor of $m \cong 0.7$. One key feature presented for these models is the modeling of the nonstationary behavior of the channel taps using the persistence process. The persistence processes have been modeled using a first-order Markov chain, and the transition and steady-state probability matrices were provided.

REFERENCES

[1] A. Jahn, M. Holzbock, J. Müller, R. Kebel, M. de Sanctis, A. Rogoyski, E. Trachtman, O. Franzrahe, M. Werner, and F. Hu, "Evolution of aeronautical communications for personal and multimedia services," *IEEE Commun. Mag.*, vol. 41, no. 7, pp. 36–43, Jul. 2003.

[2] D. W. Matolak, I. Sen, and W. Xiong, "The 5-GHz airport surface area channel—Part I: Measurement and modeling results for large airports," *IEEE Trans. Veh. Technol.*, vol. 57, no. 4, pp. 2014–2026, Jul. 2008.

[3] NASA ACAST. (2006, Jul. 17). [Online]. Available: http://acast.grc.nasa.gov/

[4] B-VHF. (2006, Jul. 16). [Online]. Available:http://www.b-vhf.org/b-vhf/

[5] FCC Auctions Homepage. (2006, Jul.). [Online]. Available: http://wireless.fcc.gov/auctions/

[6] P. Bello, "Characterization of randomly time-variant linear channels," *IEEE Trans. Commun.*, vol. COM-11, no. 4, pp. 360–393, Dec. 1963.

[7] P. A. Bello, "Aeronautical channel characterization, " *IEEE Trans. Commun.*, vol. COM-21, no. 5, 548–563, May 1973.

[8] J. Painter, S. Gupta, and L. Wilson, "Multipath modeling for aeronautical communications," *IEEE Trans. Commun.*, vol. COM-21, no. 5, pp. 658–662, May 1973.

[9] J. Capon, "Multipath parameter computations for the MLS simulation computer program," Lincoln Lab., Mass Inst. Technol., Lexington, MA, MIT Lincoln Lab. Tech. Rep. ATC-68, Apr. 8, 1976.

[10] E. Haas, "Aeronautical channel modeling," *IEEE Trans. Veh. Technol.*, vol. 51, no. 2, pp. 254–264, Mar. 2002.

[11] D. W. Matolak, "Wireless channel characterization in the 5 GHz microwave landing system extension band for airport surface areas," Ohio University, Athens, OH, NASA ACAST Final Project Rep., Grant NNC04GB45G, May 2006.

[12] I. Sen and D. W. Matolak, "Channel modeling for airport surface network communications: Transmission/reception from airport field sites," in *Proc. Digit. Avionics Syst. Conf.*, Portland, OR, Oct. 15–19, 2006.

[13] D. C. Cox, "910 MHz urban mobile radio propagation: Multipath characteristics in New York City," *IEEE Trans. Commun.*, vol. COM-21, no. 11, pp. 1188–1194, Nov. 1973.

[14] D. C. Cox, "Delay Doppler characteristics of multipath propagation at 910 MHz in a suburban mobile radio environment," *IEEE Trans. Antennas Propag.*, vol. AP-20, no. 5, pp. 625–635, Sep. 1972.

[15] Berkeley Varitronics, Inc. (2007, Jan.). [Online]. Available: http://www.bvsystems.com/

[16] G. Matz, A. F. Molisch, F. Hlawatsch, M. Steinbauer, and I. Gaspard, "On the systematic measurement errors of correlative mobile radio channel sounders," *IEEE Trans. Commun.*, vol. 50, no. 5, pp. 808–821, May 2002.

[17] E. S. Sousa, V. M. Jovanovic, and C. Daigneault, "Delay spread measurements for the digital cellular channel in Toronto," *IEEE Trans. Veh. Technol.*, vol. 43, no. 4, pp. 837–847, Nov. 1994.

[18] G. Stuber, *Principles of Mobile Communications*. Norwell, MA: Kluwer, 1996.

[19] G. Matz, "On non-WSSUS wireless fading channels," *IEEE Trans. Wireless Commun.*, vol. 4, no. 5, pp. 2465–2478, Sep. 2005.

[20] R. J. C. Bultitude, "Estimating frequency correlation functions from propagation measurements on fading channels: A critical review," *IEEE J. Sel. Areas Commun.*, vol. 20, no. 6, pp. 1133–1143, Aug. 2002.

[21] A. Papoulis and U. Pillai, *Probability, Random Variables, and Stochastic Processes*, 4th ed. New York: McGraw-Hill, 2001.

[22] A. F. Molisch, "Ultrawideband propagation channels—Theory, measurement, and modeling," *IEEE Trans. Veh. Technol.*, vol. 54, no. 5, pp. 1528–1545, Sep. 2005.

[23] J. B. Andersen, "Statistical distributions in mobile communications using multiple scattering," in *Proc. 27th URSI Gen. Assem.*, Maastricht, The Netherlands, Aug. 2002.

[24] D. Gesbert, H. Bolcskei, D. A. Gore, and A. J. Paulraj, "Outdoor MIMO wireless channels: Models and performance prediction," *IEEE Trans. Commun.*, vol. 50, no. 12, pp. 1926–1934, Dec. 2002.

[25] I. Sen, D. W. Matolak, and W. Xiong, "Wireless channels that exhibit 'worse than Rayleigh' fading: Analytical and measurement results," in *Proc. MILCOM*, Washington, DC, Oct. 23–25, 2006, pp. 1–7.

[26] ITT Industries, Inc., *Technology Assessment for the Future Aeronautical Communication System*, Jul. 2006.

[27] IEEE Stand. Assoc. (2006, Jul. 3). 802.16 website. [Online]. Available: http://standards.ieee.org/getieee802/802.16.html

[28] ITU document Rec. ITU-R M.1225, *Guidelines for Evaluation of Radio Transmission Technologies for IMT-2000 Systems*, 1998.

[29] J. Kivinen, X. Zhao, and P. Vainikainen, "Empirical characterization of wideband indoor radio channel at 5.3 GHz," *IEEE Trans. Antennas Propag.*, vol. 49, no. 8, pp. 1192–1203, Aug. 2001.

[30] R. L. Peterson, R. E. Ziemer, and D. E. Borth, *Introduction to Spread Spectrum Communications*. Upper Saddle River, NJ: Prentice-Hall, 1995.

Indranil Sen (M'03) was born in Mumbai, India, and received the B.E. degree from Mumbai University in 2002 and the M.S. and Ph.D. degrees from Ohio University, Athens, in 2004 and 2007, respectively, both in electrical engineering.

He is currently with the Corporate Technology Office, Motorola, Libertyville, IL. His research interests include spread spectrum communication, multicarrier waveform design, and channel modeling.

David W. Matolak (M'83–SM'00) was born in Johnstown, PA. He received the B.S. degree from The Pennsylvania State University, University Park, in 1983, the M.S. degree from the University of Massachusetts (UMass), Amherst, in 1987, and the Ph.D. degree from the University of Virginia, Charlottesville, in 1995, all in electrical engineering.

He was with the Rural Electrification Administration, Washington, DC, from 1983 to 1985, where he worked on upgrading specialized rural telecommunication systems. From 1985 to 1986, he was with the Laboratory for Millimeter Wave Devices and Applications (LAMMDA), UMass, where he worked on the full-wave analysis, design, fabrication, and testing of planar microwave transmission lines and antennas. From 1986 to 1989, he was with the Microwave Radio Systems Development Department, AT&T Bell Laboratories, where he worked on analytical and empirical characterization of nonlinearities and their effect on quadrature amplitude modulation transmission. In 1990, he joined the Communication Systems Laboratory, University of Virginia, Charlottesville, where he focused on the analysis of trellis coding and equalization for TDMA mobile radio systems. From 1994 to 1996, he was with Lockheed Martin Tactical Communication Systems, where he was the Lead System Engineer on the development of a wireless local loop synchronous CDMA communication system. From 1996 to 1998, he was with the MITRE Corporation, where he worked on the analysis and modeling of various digital radio communication systems. He was with Lockheed Martin Global Telecommunications from 1998 to 1999, where he worked on mobile satellite communication system analysis and design. In September 1999, he joined the School of Electrical Engineering and Computer Science, Ohio University, Athens. His research interests include communication over fading channels, radio channel modeling, multicarrier transmission, and CDMA.

Dr. Matolak is a member of Eta Kappa Nu and Sigma Xi. He has served on several IEEE conference technical program committees and was also the Chair of the Geo Mobile Radio Standards Group in the Telecommunications Industries Association's Satellite Communications Division.